Optical studies of the 1.40-eV Ni center in diamond

Maria Helena Nazaré and A. J. Neves
Departamento e Centro de Física, Universidade de Aveiro, 3800 Aveiro, Portugal

Gordon Davies
Physics Department, King's College London, Strand, London WC2R 2LS, United Kingdom
(Received 29 November 1990)

Synthetic diamonds grown using a solvent catalyst that contains Ni show the 1.401-1.404 eV luminescence and absorption system. Isotope splitting data on the zero-phonon lines establish that the optical center contains one Ni atom. Uniaxial stress and Zeeman measurements are reported. We show that the optical transition is between a doubly degenerate orbital ground state (^2E), which is split by spin-orbit interaction, and a nondegenerate orbital excited state (^2A) at a defect with trigonal symmetry. An effective spin of $\frac{1}{2}$ is consistent with the Zeeman and the stress results. We propose that the center is a Ni^+, with electronic configuration ($3d^9, S=\frac{1}{2}$), distorted along a $\langle 111 \rangle$ direction.

I. INTRODUCTION

Diamond can now be made in the form of thin films of high crystallographic perfection, and as homogeneous crystals with edge lengths exceeding 10 mm. The high degree of control over the growth process allows the possibility of exploiting the unusual properties of diamond such as its transparency over a wide range of photon energies. This control requires knowledge of, and control over, the impurities present in the synthetic crystals. One source of impurities is the growth environment. Transition metals, particularly Ni, Co, Fe, and their alloys, are used as solvent catalysts when bulk diamonds are synthesized (or recrystallized). We could expect that these metals would be incorporated in the diamond but to date the only transition metal believed to enter diamond in the form of dispersed atoms is nickel. Diamonds which have been synthesized in the presence of nickel tend to show nickel-related paramagnetic resonance, plus optical absorption bands with zero-phonon lines at 1.40, 1.883, 2.51, and 3.1 eV, and also a broad band centered near 1.4 eV.[1] The 1.40-eV zero-phonon lines and zero-phonon lines near 2.56 eV may also be seen in luminescence spectra from diamonds synthesized in the presence of nickel and can also be seen from diamonds which have been implanted with Ni ions.[2,3] Recently we have unambiguously demonstrated that Ni is responsible for the 1.40-eV lines by detecting the effects of the different isotopes of nickel.[4] Consequently the 1.40-eV center is the only optical center which at present is known unambiguously to be caused by a transition metal. It is timely to investigate this optical center in some detail, and this is the purpose of the present paper.

The paper is organized as follows. The 1.40-eV zero-phonon lines consist of a doublet, at 1.401 and 1.404 eV. The widths of these lines in our diamonds are considerably smaller than previously reported by earlier workers. In Sec. III we exploit this small linewidth to make accurate measurements of the temperature variations of the lines, confirming that all the doublet splitting is in the ground state of the optical transition. Each component of the doublet is shown, in Sec. IV, to have fine structure which we establish is caused by the different isotopes of natural nickel the effects being produced by only one Ni atom per center. Conceptually, the simplest site occupied by one Ni atom is as a substitutional atom, or in the tetrahedral interstitial cavity. However, in synthetic diamond the 1.40-eV transitions are dichroic, giving different strengths of absorption and luminescence when the angle of the polarization of the light is changed relative to a (111) growth plane.[5] The simple tetrahedral configurations are immediately excluded since these would necessarily produce isotropic transitions in the cubic lattice. Further, during the crystal growth, the centers must be nonrandomly distributed between the axes which would be equivalent in a perfectly cubic crystal. To determine the center's symmetry we have used two techniques, applying either uniaxial compressions or magnetic fields in turn along each of the three major crystallographic axes. In both measurements the perturbation lifts the equivalence of different axes in the crystal, and different components in the spectra can be identified with different orientations of centers in the crystal. The uniaxial stress results, presented in Sec. V, show that the energies of the stress-split components as functions of the applied stress are consistent with the 1.40-eV center having a trigonal symmetry. Because uniaxial stresses change the relative positions of the atoms in a optical center, they perturb only the spatial parts of the electronic states and give no information about the spin states. Direct information on the spins of the eigenstates of the center comes from magnetic perturbations. We show in Sec. VI that the center has a spin of $\frac{1}{2}$, the ground-state splitting coming from the spin-orbit interaction. The Zeeman measurements also confirm the symmetry of the optical center. We have drawn attention to the di-

chroism of the optical transitions. Using the results of this paper these effects can be explained quantitatively from unequal populations of the different trigonal orientations in the crystal (Sec. VII). Also in Sec. VII we tabulate the intensities of the stress-split components in the case of Γ_4 to Γ_4 and of Γ_5 to Γ_4 transitions at a trigonal center, point group C_3^*, and use the results to definitively identify the 1.401- and 1.404-eV lines with transitions between, respectively, two Γ_4 states and between a Γ_5 and a Γ_4 state at a trigonal center. Variations in the splittings of the doublet, including different splittings in the same sample when observed in luminescence and absorption, are explained in Sec. VIII where the paper is also summarized.

II. EXPERIMENTAL PROCEDURE

The samples used in this work were synthetic diamond grown by De Beers Diamond Research Laboratory using a nickel-iron solvent catalyst. For the uniaxial stress and Zeeman measurements, they were polished into cuboids, with (111), $(1\bar{1}0)$, and $(11\bar{2})$ faces and (001), (110), and $(1\bar{1}0)$ faces.

Absorption measurements were made using a 100-W quartz-halogen tungsten lamp. Luminescence was excited using a krypton ion laser, and was collected at right angles to the axis of excitation. In both cases measurements were made using Spex 1701 dispersive monochromators, fitted with either a North Coast EO-817 germanium detector or an extended-red-sensitive photomultiplier tube. Uniaxial stresses were applied using push rods driven by oil pressure, the samples being cooled by liquid nitrogen or liquid helium. The Zeeman measurements were carried out in the Voigt configuration with the samples suspended in the variable-temperature enclosure of an Oxford Instruments SpectraMag superconducting magnet.

III. ZERO-PHONON LINES: DOUBLET PROPERTIES

Cathodoluminescence from the 1.40-eV zero-phonon lines was first reported by Dean[6] using synthetic diamonds. Two zero-phonon lines were detected at 1.401 and 1.404 eV (as in the better resolved spectra of Fig. 1). Previous studies of the lines have been limited by the large linewidths of the diamonds used, caused by the relatively poor quality of the diamonds. In some cases this leads to a gross asymmetry in the properties of the lines: Collins and Spear[2] report that in one of their samples the zero-phonon lines were separated by 3.3 meV and were 3 meV wide when observed in absorption but in cathodoluminescence the separation was 2.9 meV and the width 0.8 meV. These effects may be understood quantitatively using data presented in this paper, as shown in Sec. VIII.

Figure 1 shows that both the 1.401- and 1.404-eV lines are multiplets, with the same fine structure. In luminescence the ratio of the intensities of the total multiplet structure at 1.401 eV to that at 1.404 eV is independent of temperature. In absorption their intensities vary with temperature [as shown in Figs. 2(a) and 2(b)]. Previous measurements[2] of the temperature dependence of the intensity ratio were carried out in diamonds where the 1.401- and 1.404-eV lines were not resolved. In our samples each component of the doublet was resolved, into four lines each 0.16 meV wide and with a separation between the doublet components of 2.8 ± 0.1 meV both in absorption and luminescence. Using these better samples

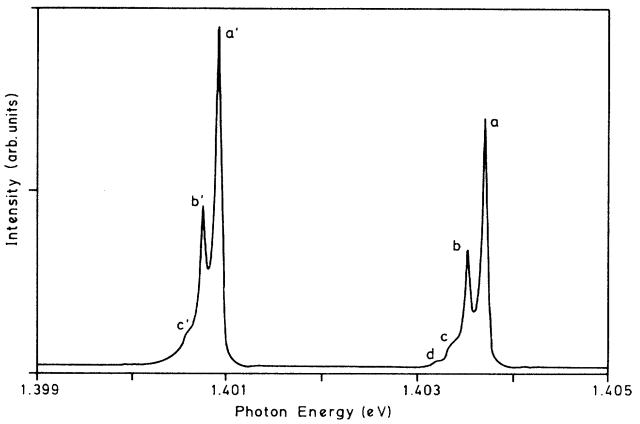

FIG. 1. The photoluminescence spectrum of a synthetic diamond recorded at 2 K showing the 1.40-eV zero-phonon doublet. Labeling is as in Table I.

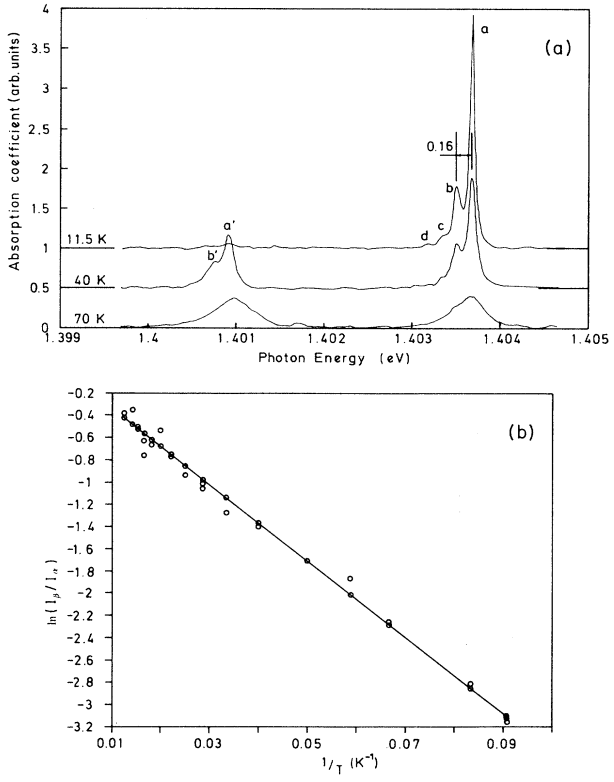

FIG. 2. (a) The 1.40-eV zero-phonon doublet recorded in absorption at three different temperatures. The fine structure is labeled as in Table I. (b) Logarithm of the intensity ratio of 1.401-1.404 eV line as a function of reciprocal temperature. Solid line represents Eq. (1) using $\Delta E = 2.80$ meV and $\alpha = 1$. These values are the best fit values in a least-squares sense.

we have remeasured the intensity ratio as a function of temperature. Figure 2(b) confirms that the intensity variation obeys a Boltzmann distribution law

$$\frac{I_{1.401}}{I_{1.404}} = \alpha \exp(-E/kT) \ . \quad (1)$$

A least-squares fit gives $E = 2.80 \pm 0.1$ meV, equal to the observed spectroscopic splitting. It appears that all the splitting of the transition occurs in its ground state. The factor α is not determined in the measurements since it is affected by the dichroism effects.

IV. ZERO-PHONON LINES: FINE STRUCTURE

Figures 1 and 2(a) show the 1.401- and 1.404-eV zero-phonon lines, taken in luminescence and absorption, respectively. The fine structure present in the lines has the same relative intensities at different temperatures when measured either in absorption or in luminescence. The fine-structure lines are equispaced, with a line separation of 0.16 meV as listed in Table I. The data for this table have been derived primarily from absorption measurements at 11 K supplemented by luminescence measurements at 2 K for the 1.401-eV line which is frozen out in absorption at low temperature.

The fine structure in each of the doublet components spans ~ 0.6 meV. If the fine structure arises from a split excited state the relative intensities of the two main components in the luminescence spectra would change by a factor of 2 when the temperature increases from 2 to 10 K. This change is definitely not observed—the states responsible for the fine structure cannot come into thermal equilibrium. The simple explanation is that each fine-structure component occurs at a different optical center, and is produced by the different isotopes of nickel.

Natural nickel has five isotopes in the abundance ratios

$$[^{58}\mathrm{Ni}]:[^{60}\mathrm{Ni}]:[^{61}\mathrm{Ni}]:[^{62}\mathrm{Ni}]:[^{64}\mathrm{Ni}] = 67.76:26.16:1.25:3.65:1.16 \ . \quad (2)$$

Figure 3 shows a reconstruction of the higher-energy line, assuming that the fine structure is produced by the isotope splitting, and that each increase of mass by one unit produces a shift of -0.08 meV in the zero-phonon energy, e.g., $h\nu^{58} - h\nu^{60} = 0.16$ meV. We have taken the shape of each isotope-split zero-phonon line to be described by

$$I(\nu) = \frac{A}{[B + (\nu - \nu_0)^2]^2} \ , \quad (3)$$

where A and B parametrize the intensity and width. The fit in Fig. 3 assumes that the isotope effect is produced by the effects of only one nickel atom per optical center. The implication is that there is probably only one Ni atom per center, but isotope studies can only establish a lower limit to the number of impurity atoms per center.

V. UNIAXIAL STRESS PERTURBATION

A. Experimental data

A closer examination of polarized absorption and cathodoluminescence measurements[5] reported by earlier workers might suggest that the 1.40-eV center has a C_3 axis and that the ground-state splitting is due to spin-orbit interaction. Furthermore, they are consistent with a nonrandom distribution of optical centers along the C_3 axes.

Compressive stresses of up to 2 GPa have been applied along the ⟨001⟩, ⟨111⟩, and ⟨110⟩ axes of synthetic diamonds. The 1.401- and 1.404-eV zero-phonon lines respond to uniaxial stress as shown in Figs. 4 and 5. Data were taken in photoluminescence. Because our sample oriented along one ⟨111⟩ axis had a nonrandom distribution of optical centers, with defects aligned mostly in one [111] direction, data for stresses along this direction are simplified. The stress-split component produced by the defects with their C_3 axes along the other [111] directions is extremely weak for both lines. We

TABLE I. Isotopic structure of 1.40-eV zero-phonon lines. Labeling is that of Fig. 1 for luminescence and of Fig. 2 for absorption.

Energy (eV)	Full width (meV)	Assigned isotope	Label	Remarks
1.403 76	0.06	58	a	Data taken
1.403 59	0.07	60	b	in absorption
1.403 43		61+62	c	at 11 K
1.403 27		64	d	
1.400 96	0.15	58	a′	Data taken
1.400 79		60	b′	in absorption
1.400 63		61+62	c′	at 20 K
1.403 68	0.07	58	a	Data taken in
1.403 51	0.06	60	b	luminescence
1.403 35		61+62	c	at 2 K
1.403 19		64	d	
1.400 88	0.08	58	a′	Data taken in
1.400 72	0.07	60	b′	luminescence
1.400 56		61+62	c′	at 2 K

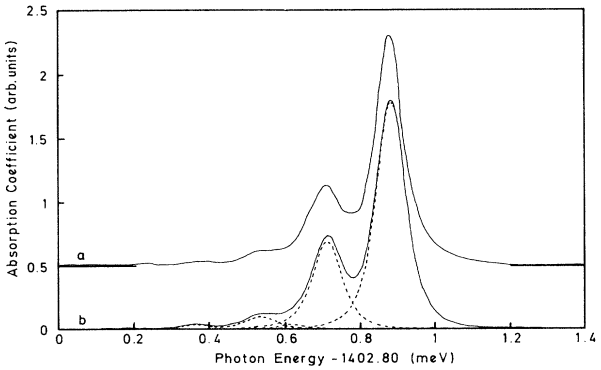

FIG. 3. Reconstruction of the shape of the 1.404-eV line using the isotope model described in Sec. IV: (a) experimental curve, (b) theoretical curve. Dashed lines show the computed line shape for each component of the 1.404-eV transition using Eq. (3).

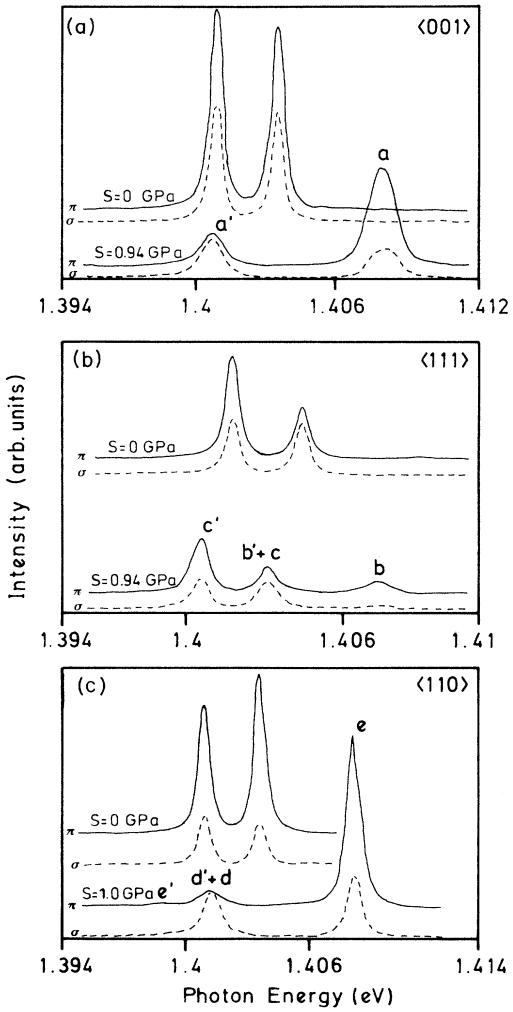

FIG. 4. The effect of uniaxial compression on the 1.40-eV zero-phonon doublet recorded in photoluminescence at 4 K. Solid and dashed lines are for π and σ polarizations, respectively. Data taken under compression along (a) ⟨001⟩; (b) ⟨111⟩; and (c) ⟨110⟩ axis.

show next that the full set of data is consistent with both the 1.401- and the 1.404-eV lines being transitions from a ^2E ground state to a ^2A excited state in a center of trigonal symmetry,[7] point group C_{3v}, D_3 or D_{3d}. The ground ^2E state is split by spin-orbit interaction, producing the doublet spacing of $\lambda = 2.80$ meV.

B. Analysis

To fix the notation we consider one specific orientation of the trigonal centers. For this orientation we define a set of local axes for the defect as follows, the Z axis parallel to the C_3 axis along [111], and the X and Y axes along $[11\bar{2}]$ and $[1\bar{1}0]$, respectively. The C_3 axis is the quanti-

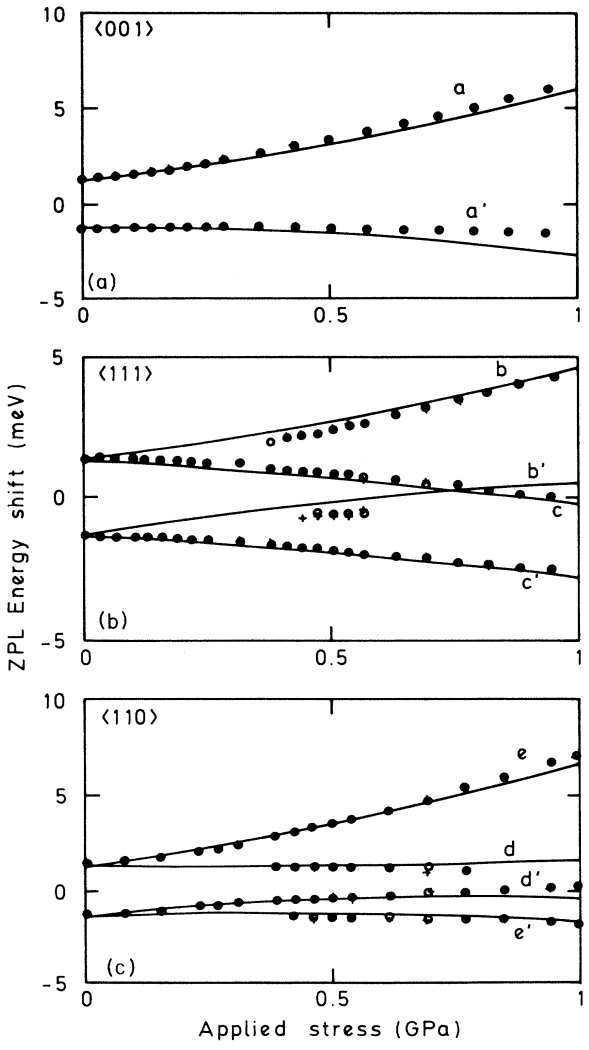

FIG. 5. A comparison of theory and experiment for the energies of the 1.401- and 1.404-eV lines under uniaxial compression along (a) ⟨001⟩; (b) ⟨111⟩; and (c) ⟨110⟩. The data measured in π polarization are shown by crosses and in σ polarization by circles. The solid lines show best fit obtained using the theory of Sec. V with the coefficients listed in the text. They are labeled according to Fig. 4.

zation axis. Using this set as the standard orientation of the trigonal defect we write the effective stress Hamiltonian as

$$H=C_{A1}(S_{XX}+S_{YY}+S_{ZZ})+\tfrac{1}{2}C'_{A1}(2S_{ZZ}-S_{XX}-S_{YY}) +C_{E\theta}(S_{YY}-S_{XX})+2C_{E\epsilon}S_{XY}+2C'_{E\theta}S_{XZ} +2C'_{E\epsilon}S_{YZ} . \quad (4)$$

Here $S_{XX},\ldots,S_{ZX}$ are stress tensor components with respect to the local axes and $C_{A1},\ldots,C'_{E\epsilon}$ electronic operators that transform, in the trigonal point group, as shown by the subscripts. Each combination of the stress tensor components transforms in the same way as the related operator, we define

$$\begin{aligned} &s_{A1}=S_{XX}+S_{YY}+S_{ZZ} ,\\ &s'_{A1}=2S_{ZZ}-S_{XX}-S_{YY} ,\\ &s_\theta=S_{YY}-S_{XX},\quad s_\epsilon=2S_{XY} ,\\ &s'_\theta=2S_{XZ},\quad s'_\epsilon=2S_{YZ} . \end{aligned} \quad (5)$$

The effective spin-orbit Hamiltonian is

$$H_{\text{s.o.}}=\xi(\mathbf{L}\cdot\mathbf{S}) . \quad (6)$$

The ^2E ground state can be written as a product of a spatial part which transforms as the E irreducible representation of the trigonal point groups and a spin part denoted as $|\alpha\rangle$ and $|\beta\rangle$. The eigenvalues and eigenfunctions of the spin-orbit secular matrix are

$$+\tfrac{1}{2}\lambda\begin{cases}|\psi_1\rangle=|E_x\alpha\rangle+i|E_y\alpha\rangle\\ |\psi_2\rangle=|E_x\beta\rangle-i|E_y\beta\rangle\end{cases} \quad (7)$$

$$-\tfrac{1}{2}\lambda\begin{cases}|\psi_3\rangle=|E_x\alpha\rangle-i|E_y\alpha\rangle\\ |\psi_4\rangle=|E_x\beta\rangle+i|E_y\beta\rangle\end{cases} . \quad (8)$$

In this basis set the secular matrix which describes the effect of the stress induced perturbation is

$$\begin{pmatrix} \delta+\frac{1}{2}\lambda & 0 & \eta & 0\\ 0 & \delta+\frac{1}{2}\lambda & 0 & \eta\\ \eta^* & 0 & \delta-\frac{1}{2}\lambda & 0\\ 0 & \eta^* & 0 & \delta-\frac{1}{2}\lambda \end{pmatrix} , \quad (9)$$

where

$$\begin{aligned} &\delta=a_1s_{A1}+\tfrac{1}{2}a_2s'_{A1} ,\\ &\eta=-b(s_\theta+is_\epsilon)-c(s'_\theta+is'_\epsilon) , \end{aligned} \quad (10)$$

in terms of the matrix elements defined as

$$\begin{aligned} &a_1=\langle E_y\alpha,\beta|C_{A1}|E_y\alpha,\beta\rangle ,\\ &a_2=\langle E_y\alpha,\beta|C'_{A1}|E_y\alpha,\beta\rangle ,\\ &b=\langle E_y\alpha,\beta|C_{E\theta}|E_y\alpha,\beta\rangle ,\\ &c=\langle E_y\alpha,\beta|C'_{E\theta}|E_y\alpha,\beta\rangle . \end{aligned} \quad (11)$$

We note that there are no matrix elements of the stress perturbation between states of different spins. Experimentally we can only determine the differences in the responses to totally symmetric perturbations of the ground and excited states. Consequently we define an origin for the totally symmetric stress effects such that $\langle E_y\alpha,\beta|C_{A1}|E_y\alpha,\beta\rangle$ and $\langle E_y\alpha,\beta|C'_{A1}|E_y\alpha,\beta\rangle$ stand for $\langle E_y\alpha,\beta|C_{A1}|E_y\alpha,\beta\rangle-\langle A\alpha,\beta|C_{A1}|A\alpha,\beta\rangle$ and $\langle E_y\alpha,\beta|C'_{A1}|E_y\alpha,\beta\rangle-\langle A\alpha,\beta|C'_{A1}|A\alpha,\beta\rangle$, respectively.

For each direction of the applied stress and each orientation of the trigonal defect the secular matrix of Eq. (9) can be diagonalized, yielding the corresponding perturbation to the zero-stress energy difference between the excited and fundamental states of the transitions. A comparison between the experimental energies for every stress split component and the corresponding values calculated using this model is shown in Fig. 5. The lines on Fig. 5 have been calculated with the best fit value for the stress parameters, Eq. (11), of

$$a_1=1.6,\quad a_2=-3.0,\quad b=3.2,\quad c=2.1 , \quad (12)$$

all in meV GPa^{-1} and closely fit the data. The quality of the fit confirms that the doublet originates at a trigonal center, between ^2E and ^2A states, the former being spin-orbit split.

To understand the intensity of each stress-split component we need to take into account the nonrandom distribution of optical centers; that is done quantitatively in Sec. VII.

VI. ZEEMAN RESULTS

A. Experimental data

Magnetic fields up to 6 T have been applied along the ⟨001⟩, ⟨111⟩, and ⟨110⟩ axes of synthetic diamonds. The 1.40-eV doublet responds to the applied field as shown in Figs. 6 and 7. Data were taken at 4 K in photoluminescence. The samples used were the same as in the stress experiment and consequently, again the data for fields along ⟨111⟩ reflect the nonrandomly distribution of defects; the splitting due to orientational degeneracy is not present since only one [111] direction is populated [Fig. 6(b)]. The data are consistent with both the 1.40-eV lines occuring at a center of trigonal symmetry. The spin degeneracy of 2 is confirmed by the Zeeman results and also the orbital assignment of the states involved.

B. Analysis

The perturbation to the Hamiltonian due to the magnetic field can, in this case of a trigonal defect, be described by

$$\Delta H=\beta(g_1B_XS_X+g_1B_YS_Y+g_3B_ZS_Z) , \quad (13)$$

where β is the Bohr magneton and the quantization axis is the Z trigonal axis of the center.

The energy separation between the excited and ground states is large enough to allow us to ignore any interactions induced by the magnetic field between these states.

Therefore, we analyze the effects of the applied magnetic field on the fundamental and excited states separately and define

$$g_1(B_X - iB_Y) = \langle \psi_1 | \Delta H | \psi_4 \rangle, \quad g_3 = \langle \psi_1 | \Delta H | \psi_1 \rangle , \quad g_3' = \langle \psi_3 | \Delta H | \psi_3 \rangle , \tag{14}$$

$$g_1^e(B_X - iB_Y) = \langle A\alpha | \Delta H | A\beta \rangle, \quad g_3^e = \langle A\alpha | \Delta H | A\alpha \rangle . \tag{15}$$

The secular matrix describing the magnetic perturbation on the fundamental states of the 1.401- and 1.404-eV doublet is

$$\begin{bmatrix} g_3 B_Z + \frac{1}{2}\lambda & 0 & 0 & g_1 B_X - i g_1 B_Y \\ 0 & -g_3 B_Z + \frac{1}{2}\lambda & g_1 B_X - i g_1 B_Y & 0 \\ 0 & g_1 B_X + i g_1 B_Y & g_3' B_Z - \frac{1}{2}\lambda & 0 \\ g_1 B_X + i g_1 B_Y & 0 & 0 & -g_3' B_Z - \frac{1}{2}\lambda \end{bmatrix} \tag{16}$$

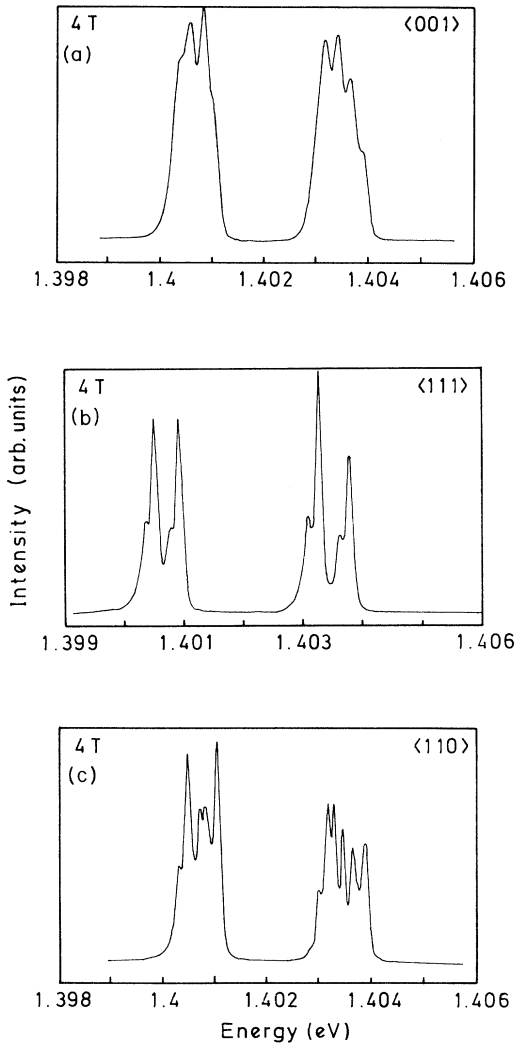

FIG. 6. Photoluminescence spectra recorded at 4 K showing the effect of an applied magnetic field on the 1.40-eV zero-phonon doublet. Data taken under a magnetic field along (a) ⟨001⟩, (b) ⟨111⟩, (c) ⟨110⟩ axis.

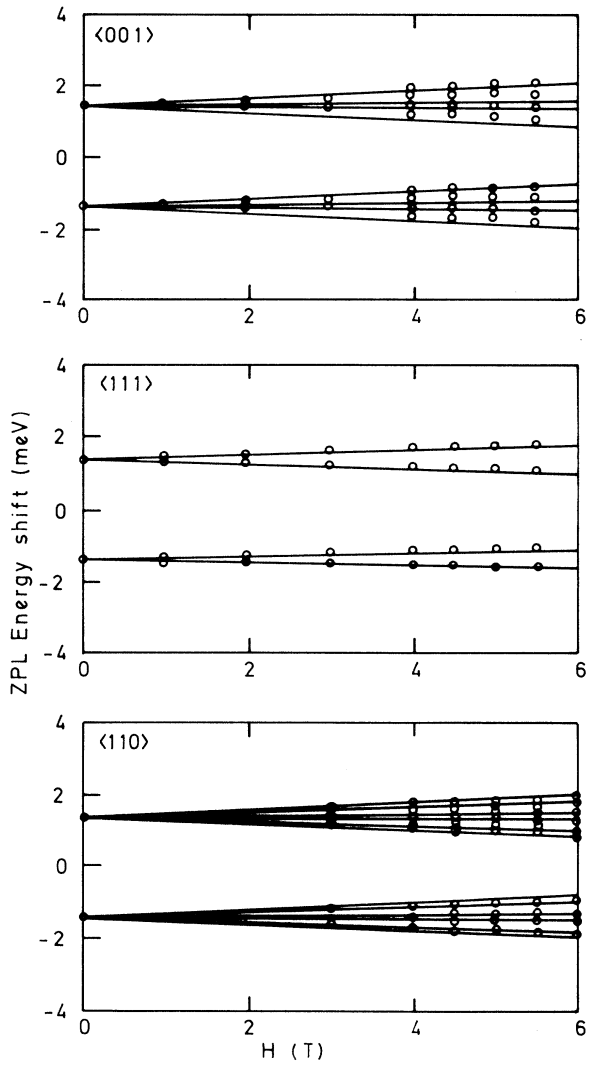

FIG. 7. A comparison of theory and experiment for the energies of the 1.401 and 1.404 eV lines under a magnetic field along (a) ⟨001⟩; (b) ⟨111⟩; and (c) ⟨110⟩. The solid lines show best fit obtained using the theory of Sec. VI with the coefficients listed in Eq. (18).

ordered in the basis set $|\psi_1\rangle$, $|\psi_2\rangle$, $|\psi_3\rangle$, and $|\psi_4\rangle$ of Eqs. (7) and (8). The secular matrix for the excited state is

$$\begin{bmatrix} g_3^e B_Z & g_1^e B_X - i g_1^e B_Y \\ g_1^e B_X + i g_1^e B_Y & -g_3^e B_Z \end{bmatrix} \tag{17}$$

in the $|A\alpha\rangle, |A\beta\rangle$ states.

We note that the magnetic field completely removes the degeneracy in the excited as well as in the ground state; it also induces interactions between the $|\psi_{1,2}\rangle$ and $|\psi_{4,3}\rangle$ states and between the $|A\alpha\rangle$ and $|A\beta\rangle$ states.

For each direction of the applied magnetic field and each orientation of the trigonal defect, the secular matrix for the fundamental and excited states can be diagonalized. The energy of a split component is given by the difference between every eigenvalue of the secular matrix for the excited state and for the fundamental state. The results are shown in Fig. 7. The lines on Fig. 7 have been calculated with the best-fit value for the effective g factors, of Eqs. (14) and (15),

$$\begin{aligned} &g_1 = \pm 0.64, \quad g_3 = 1.21, \quad g_3' = 0.81 , \\ &g_1^e = 1.25, \quad g_3^e = \pm 0.09 . \end{aligned} \tag{18}$$

The data are closely fit, confirming that the optical center has a trigonal symmetry and a spin of $\frac{1}{2}$.

VII. DICHROISM OF THE OPTICAL TRANSITIONS

Recently attention has been drawn to the strong localization of the 1.40-eV optical centers in the {111} growth sectors of diamond. In many samples, the 1.40-eV absorption and luminescence are strongly polarized with respect to the ⟨111⟩ axis. In particular, Collins[5] reports that the degree of polarization along one [111] axis is not the same for both components of the doublet. Specifically, in measurements carried out in absorption and cathodoluminescence, the high-energy component at 1.404 eV was almost 100% polarized, with **E** vector parallel to the {111} growth planes, while the intensity of the 1.401-eV component varied only about 30%.

A photoluminescence spectrum obtained from our sample oriented with (111), (1$\bar{1}$0), and (11$\bar{2}$) faces, used in this work, is shown in Fig. 8, and in that the different degree of polarization of the two components can be clearly seen.

We will show that both the dichroism and the different degree of polarization exhibited by the doublet components can be quantitatively accounted for, in terms of an allowed dipole transition occuring at a trigonal center, between a spin-orbit split ground state, and an orbitally nondegenerate excited state, if a nonrandom distribution of optical centers is invoked.

A. Analysis

In the absence of spin-orbit interaction the ^2E ground states which are degenerate transform under the symmetry operations of the trigonal group as the product of $\Gamma_3 \otimes \Gamma_4$ representations of the double group C_{3v}^* while the ^2A excited states transform as the $\Gamma_1 \otimes \Gamma_4$ product in the same point group. Transitions between these states are allowed for X, Y, and Z dipoles. Using the standard basis $|lm\rangle|sm_s\rangle$ associated with a fictitious effective angular orbital momentum $\tilde{l}=1$ and a spin of $\frac{1}{2}$ the behavior of the ^2E ground state in the trigonally distorted environment can be described in terms of the E irreducible representation and the spin part as

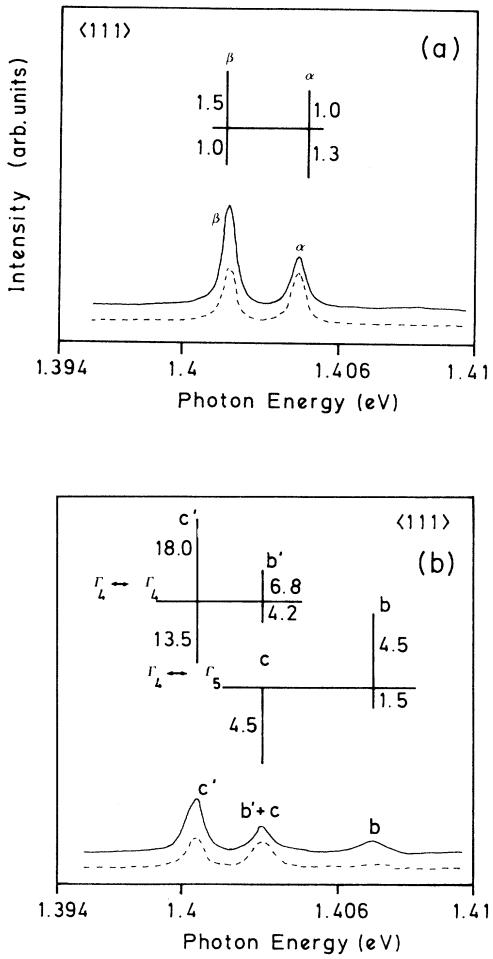

FIG. 8. (a) Photoluminescence spectrum recorded at 4 K. Luminescence was collected at right angles with the excitation direction. Solid line and dashed lines are for light polarized parallel and perpendicular to the ⟨111⟩ direction, respectively. Spike spectra give calculated intensities with theory of Sec. VII (assuming that $\frac{3}{4}$ of the centers have their C_3 axis along [111] and the remaining quarter are distributed along any of the other possible directions). Labeling is that of Eq. (23) and of Table II. (b) The effect of uniaxial compression on the 1.40-eV zero-phonon doublet recorded in photoluminescence at 4 K. Solid line is for π and dashed line for σ polarizations. Data taken under compression along ⟨111⟩. Spike spectra give calculated intensities with theory of Sec. VII. Labeling is that of Table III and of Fig. 4(b).

$$
\begin{aligned}
|E_x\alpha\rangle &= \frac{1}{\sqrt{2}}(-|11\rangle+|1\bar{1}\rangle)|\tfrac{1}{2}\tfrac{1}{2}\rangle\ , \\
|E_x\beta\rangle &= \frac{1}{\sqrt{2}}(-|11\rangle+|1\bar{1}\rangle)|\tfrac{1}{2}\,\bar{\tfrac{1}{2}}\rangle\ , \\
|E_y\alpha\rangle &= \frac{i}{\sqrt{2}}(|11\rangle+|1\bar{1}\rangle)|\tfrac{1}{2}\tfrac{1}{2}\rangle\ , \\
|E_y\beta\rangle &= \frac{i}{\sqrt{2}}(|11\rangle+|1\bar{1}\rangle)|\tfrac{1}{2}\,\bar{\tfrac{1}{2}}\rangle\ .
\end{aligned}
\tag{19}
$$

In the same way the excited ^2A state can be described as

$$
|A\alpha\rangle = |10\rangle|\tfrac{1}{2}\tfrac{1}{2}\rangle
$$

and

$$
|A\beta\rangle = |10\rangle|\tfrac{1}{2}\,\bar{\tfrac{1}{2}}\rangle\ . \tag{20}
$$

Spin-orbit interaction splits the ground state, as described in Eqs. (7) and (8), into Γ_4 and Γ_5 states, but does not affect the Γ_4 excited states.

To calculate the relative intensities of the doublet components at 1.404 and 1.401 eV and the respective degree of polarization it is less cumbersome to have states of Eqs. (7) and (8) written in terms of the $|jm_j\rangle$, basis states of J^2, J_z. This is easily done using the elementary vector model for addition of angular momenta and the Wigner coefficients, resulting in

$$
|\psi_1^g\rangle = |\tfrac{3}{2}\tfrac{3}{2}\rangle,\quad |\psi_2^g\rangle = |\tfrac{3}{2}\,\bar{\tfrac{3}{2}}\rangle\ , \tag{21}
$$

transforming as the degenerate Γ_5 representation of the C_{3v}^* double group and

$$
\begin{aligned}
|\psi_3^g\rangle &= \sqrt{1/3}|\tfrac{3}{2}\,\bar{\tfrac{1}{2}}\rangle - \sqrt{2/3}|\tfrac{1}{2}\,\bar{\tfrac{1}{2}}\rangle\ , \\
|\psi_4^g\rangle &= \sqrt{1/3}|\tfrac{3}{2}\tfrac{1}{2}\rangle + \sqrt{2/3}|\tfrac{1}{2}\tfrac{1}{2}\rangle\ ,
\end{aligned}
\tag{22}
$$

transforming as the Γ_4 representation of the same C_{3v}^*.

We denote transitions $|\psi_1^g\rangle, |\psi_2^g\rangle \leftrightarrow |\psi_1^e\rangle, |\psi_2^e\rangle$ and $|\psi_3^g\rangle, |\psi_4^g\rangle \leftrightarrow |\psi_1^e\rangle, |\psi_2^e\rangle$ as the α and β lines, respectively. Their intensities I_α and I_β are proportional to

$$
I_\alpha \cong \sum_{i=1}^{2}\sum_{j=1}^{2} |\langle\psi_i^g|\mathbf{T}|\psi_j^e\rangle|^2
$$

and

$$
I_\beta \cong \sum_{i=3}^{4}\sum_{j=1}^{2} |\langle\psi_i^g|\mathbf{T}|\psi_j^e\rangle|^2\ , \tag{23}
$$

where $\mathbf{T}$ is a vector operator, the electric dipole of the light, with components T_z, T_x, and T_y. The determination of these matrix elements is a direct application of the Wigner-Eckart theorem giving

$$
\begin{aligned}
&|\langle\psi_1^g,\psi_2^g|\mathbf{T}_z|\psi_1^e,\psi_2^e\rangle|^2 = 0\ , \\
&|\langle\psi_3^g,\psi_4^g|\mathbf{T}_z|\psi_1^e,\psi_2^e\rangle|^2 = \tfrac{1}{2}a_\parallel^2\ , \\
&|\langle\psi_1^g,\psi_2^g|\mathbf{T}_{x,y}|\psi_1^e,\psi_2^e\rangle|^2 = \tfrac{1}{2}b^2\ , \\
&|\langle\psi_3^g,\psi_4^g|\mathbf{T}_{x,y}|\psi_1^e,\psi_2^e\rangle|^2 = \tfrac{1}{2}a_\perp^2\ .
\end{aligned}
\tag{24}
$$

We resolve the electric vector $\mathbf{d}$ of the excitation light along the X, Y, and Z axis of the trigonal defect, $\hat{\mathbf{d}} = l\hat{\mathbf{X}} + h\hat{\mathbf{Y}} + k\hat{\mathbf{Z}}$, giving

$$
\begin{aligned}
I_\alpha &\cong |(l+h)b|^2\ , \\
I_\beta &\cong |(l+h)a_\perp + ka_\parallel|^2\ .
\end{aligned}
\tag{25}
$$

For each orientation of the trigonal center the intensity of the α and β transitions was calculated. The results for excitation light polarized parallel and perpendicular to the [111] direction are listed in Table II, for the special case of $a_\parallel = a_\perp$ and $b/a = 1.0$, which is shown below to describe the present data. For a random distribution of optical centers the two transitions α and β *do not* have equal intensity. The predicted intensity ratio is $I_\alpha/I_\beta = 2/3$. Also according to this model neither transition should exhibit any degree of dichroism, either in absorption or cathodoluminescence, as expected for a random distribution of optical centers in a cubic lattice.

Now we assume that the Ni centers where the 1.4-eV transitions occur are preferentially alligned in a certain $\langle 111\rangle$ direction. We take, as an example of the nonran-

TABLE II. Intensities of α and β lines, excited by light linearly polarized parallel and perpendicular to the [111] direction. d is the electric vector of the exciting light. d' is the electric vector of the emitted light.

	Absorption				Emission[a]			
	$I_\alpha(b^2)$		$I_\beta(a^2)$		$I_\alpha(b^2)$		$I_\beta(a^2)$	
C_3 axis	$d_\parallel$	$d_\perp$	$d_\parallel$	$d_\perp$	$d'_\parallel$	$d'_\perp$	$d'_\parallel$	$d'_\perp$
[111]	0	3	3	3	0.0	1.5	6.4	4.5
[1$\bar{1}$1]	2.7	1.7	3	3	4.6	1.5	7.1	4.1
[11$\bar{1}$]	2.7	1.7	3	3	4.6	1.5	7.1	4.1
[11$\bar{1}$]	2.7	1.7	3	3	4.0	1.5	6.4	4.5
Random distribution								
Total intensity[b]	1	1	1.5	1.5	2.2	1	4.5	2.8
Nonrandom distribution: only centers with C_3 along [111]:								
Total intensity[b]	0	1	1	1	0	1	4.3	3

[a]Luminescence excited by unpolarized radiation, traveling at right angles to the detection. Intensities calculated as in Ref. 8.
[b]Normalized to minimum intensity.

dom distribution, the case where only centers with the C_3 axis along the [111] direction are present. In this case, the transition $|\psi_1^g\rangle, |\psi_2^g\rangle \leftrightarrow |\psi_1^e\rangle, |\psi_2^e\rangle$, that is the α line, should be 100% polarized, with **E** vector parallel to the {111} growth planes.

The photoluminescence spectrum of Fig. 8 was recorded from the sample with (111), $(1\bar{1}0)$, and $(11\bar{2})$ faces; the intensity ratios shown are reproduced (spike spectra in Fig. 8) using the model above with three of every four centers having the C_3 axis along the [111] direction and a quarter of the centers having their trigonal axis along any of the other three possible directions, $[11\bar{1}]$, $[1\bar{1}1]$, and $[\bar{1}11]$. To calculate the spike spectra of Fig. 8 for these photoluminescence data the active dipole of the transition has to be considered twice,[8] first relative to the exciting direction and second to the emitting direction. The comparison identifies the α line with the high-energy component of the doublet, that is, the 1.404-eV transition occurs between a Γ_5 state and a Γ_4 state. This identification is confirmed by the relative intensities exhibited by the stress-split components of both lines, as shown in the next section.

B. Intensities under uniaxial stress

The effects of uniaxial stress and spin-orbit interaction on ^2E to ^2A transitions, occuring at a trigonal center, have been already reported.[7] However, the fact that transitions are allowed for X, Y, and Z dipoles was not taken into account; it is therefore necessary to include that study here.

To calculate the relative intensities of the stress-split components, we used methods of Sec. VII A with the eigenfunctions that diagonalize the secular matrix in Eq. (9) for every direction of stress and every orientation of the trigonal defect. Results are summarized in Table III for absorption, with $a_{\parallel} = a_{\perp}$ and $b/a = 1.0$ and a random distribution of optical defects. For stresses along the $\langle 111 \rangle$ direction both lines are split into two components. We note that in the case of the β line the two stress-split components are allowed in both π and σ polarizations while for the α line only one component can be seen in π polarization.

Results expected in photoluminescence for the case of our $\langle 111 \rangle$ samples for which we have to consider a nonrandom distribution of optical defects are also included in Table III and shown in Fig. 8(b), together with experimental spectra.

We conclude that the intensities of the stress-split components are consistent with the 1.404- and 1.401-eV transitions occuring at a trigonal defect C_{3v}^* point group between a Γ_4 and a Γ_5 state and between two Γ_4 states, respectively.

VIII. SUMMARY AND CONCLUSIONS

We have demonstrated, quantitatively, that the 1.404- and 1.401-eV transitions observed in the absorption-luminescence spectra of synthetic diamond occur at a defect involving nickel. The data suggest that there is only one Ni atom per optical center.

Using samples with very low internal strains we have measured the intensity ratio of both components as a function of temperature and confirmed that the transitions originate from a split ground state.

From uniaxial stress results we have shown that the optical center has a trigonal symmetry, the electronic ground state transforms as the product $\Gamma_3 \otimes \Gamma_4$, and the excited state as $\Gamma_1 \otimes \Gamma_4$, in the trigonal double group C_{3v}^*. The ground-state degeneracy is partially lifted by spin-orbit coupling, and splits into two states transforming as Γ_4 and Γ_5.

Direct information on the electronic spins of the states involved have been deduced from magnetic perturbations. A spin of $\frac{1}{2}$ and the trigonal symmetry are consistent with the Zeeman measurements. The ground-state

TABLE III. Relative intensities of the stress-split components of (α and β lines) $\Gamma_4 \leftrightarrow \Gamma_5$ and $\Gamma_4 \leftrightarrow \Gamma_4$ transitions at a trigonal center C_{3v}^* point group.

	α line ($\Gamma_4 \leftrightarrow \Gamma_5$)		β line ($\Gamma_4 \leftrightarrow \Gamma_4$)	
Stress axis	Label	$\pi:\sigma$	Label	$\pi:\sigma$
[001]	a	8:8	a′	12:12
[111]	b	0:3	b′	3:3
	c	8:5	c′	9:9
		$\pi:\sigma_{001}:\sigma_{1\bar{1}0}$		$\pi:\sigma_{001}:\sigma_{1\bar{1}0}$
[110]	d	6:4:2	d′	6:6:6
	e	2:4:6	e′	6:6:6
Results expected for luminescence with a random distribution				
[111]	b	13.4:4.5	b′	20.6:12.7
	c	0.0:1.5	c′	6.0:4.5
Results expected for luminescence with a nonrandom distribution[a]				
[111]	b	4.5:1.5	b′	6.8:4.2
	c	0.0:4.5	c′	18.0:13.5

[a] $\frac{3}{4}$ of the centers having the C_3 axis along the [111] direction and $\frac{1}{4}$ distributed equally with the C_3 axis along any of the other three possible directions $[11\bar{1}]$, $[1\bar{1}1]$, or $[\bar{1}11]$.

splitting coming from the spin-orbit interaction is consistent with both the Zeeman and the stress data.

Our results show that one effect of the uniaxial stress perturbations is to increase the mean splitting of the zero-phonon lines (Fig. 5). This explains the variation in the splitting which has been reported by other workers,[2] with splittings of 2.9–3.3 meV being observed, the splitting increasing with increasing linewidths (caused by increasing internal strains).

We explained quantitatively the dichroism exhibited by the optical transitions and the different degree of polarization exhibited by the two components of the doublet in terms of a nonrandom distribution of optical centers. The relative intensities and polarizations of the stress-split components were tabulated for stresses along the three major crystalographic directions, [001], [111], and [110].

This result used together with the stress and Zeeman results establishes that 1.404- and 1.401-eV transitions occur at a trigonal defect C_{3v}^{*} point group between a Γ_4 and a Γ_5 state and between two Γ_4 states, respectively.

Recently using electron paramagnetic resonance techniques a tetrahedral center with $g=2.0319$ and effective spin of $\frac{3}{2}$, has been found in synthetic diamonds, grown in the presence of nickel without nitrogen getters.[9] The center has been identified with a Ni^{-} with electronic configuration ($3d^7$), and a correlation between the number of such centers and the absorption line at 2.51 eV has been reported.[10] The 1.401-1.404 eV defect is strong in samples with a low nitrogen concentration contrary to what happens with the 2.51-eV band.

The results reported in the present paper are consistent with a spin of $\frac{1}{2}$ and a trigonal symmetry for the Ni defect where the 1.401-1.404 eV optical transitions occur. It is likely that such defect is an interstitial Ni^{+} atom in a ($3d^9$) electronic configuration distorted along a $\langle 111 \rangle$ direction. Cluster model calculations recently reported by Paslovsky and Lowther[11] show that interstitial Ni^{+} is a candidate to account for the symmetry of the states involved and also explain the origin of the spin-orbit interaction on the ground state.

Another two paramagnetic centers NIRIM-1 and NIRIM-2 have just been reported[12] to occur in synthetic diamond. The NIRIM-2 center is tentatively associated with the 1.401-1.404 eV optical defect studied in this paper.

ACKNOWLEDGMENTS

We thank R. J. Caveney and G. J. Davies for providing the specimens, and M. Seal for preparing them. We acknowledge Professor E. C. Lightowlers for assistance with experiments. The work was financed partly by Instituto Nacional de Investigacão Científica (INIC and Junta Nacional de Investigacão Científica e Tecnológica (JNICT). We also thank INIC for support for A.N.

[1] A. T. Collins, H. Kanda, and R. C. Burns, Philos. Mag. B **61**, 797 (1990).
[2] A. T. Collins and M. P. Spear, J. Phys. C **16**, 963 (1983).
[3] A. A. Gippius, V. S. Vavilov, A. M. Zaitsev, and B. S. Zhakupbekov, Physica **116B**, 187 (1983).
[4] G. Davies, A. J. Neves, and M. H. Nazaré, Europhys. Lett. **9**, 47 (1989).
[5] A. T. Collins, J. Phys. Condens. Matter **1**, 439 (1989).
[6] P. J. Dean, Phys. Rev. **139**, A588 (1965).
[7] I. K. Ludlow, J. Phys. C **1**, 1194 (1968).
[8] M. H. Nazaré, Europhys. Lett. **4**, 73 (1987).
[9] J. Isoya, H. Kanda, J. R. Norris, J. Tang, and M. K. Bowman, Phys. Rev. B **41**, 3905 (1990).
[10] H. Kanda, J. Isoya, and A. T. Collins (unpublished).
[11] L. Paslovsky and J. E. Lowther (private communication).
[12] J. Isoya, H. Kanda, and Y. Uchida, Phys. Rev. B **42**, 9843 (1990).